An active role of extratropical sea surface temperature anomalies in determining anomalous turbulent heat flux

Youichi Tanimoto

Frontier Research System for Global Change, Yokohama, Japan and Graduate School of Environmental Earth Science, Hokkaido University, Sapporo, Japan

Hisashi Nakamura

Frontier Research System for Global Change, Yokohama, Japan and Department of Earth and Planetary Science, University of Tokyo, Tokyo, Japan

Takashi Kagimoto and Shozo Yamane

Frontier Research System for Global Change, Yokohama, Japan

Abstract. Temporal and spatial structures of turbulent latent and sensible heat flux anomalies are examined in relation to dominant patterns of sea surface temperature anomalies (SSTA) observed over the North Pacific. Relative importance among observed anomalies in SST, surface air temperature and wind speed in determining the anomalous turbulent heat fluxes is assessed through linearizing the observed flux anomalies. Over the central basin of the North Pacific, changes in the atmospheric variables, including air temperature and wind speed, are primarily responsible for the generation of local SST variations by changing turbulent heat flux, which supports a conventional view of extratropical air-sea interaction. In the region where ocean dynamics is very important in forming SSTAs, in contrast, SSTAs that have been formed in early winter play the primary role in determining mid- and late-winter turbulent heat flux anomalies, indicative of the SST forcing upon the overlying atmosphere. Specifically, both decadal scale SSTAs in the western Pacific subarctic frontal zone and El Niño related SSTAs south of Japan are found to be engaged actively in such forcing on the atmosphere. The atmospheric response to this forcing appears to include the anomalous storm track activity. The observed atmospheric anomalies, which may be, in part, forced by the preexisting SSTAs in those two regions, act to force SSTAs in other portions of the basin, leading to the time evolution of SSTAs as observed in the course of the winter season.

1. Introduction

As a thermal boundary condition for persistent atmospheric circulation anomalies, it is of certain importance to capture spatial and temporal characteristics of sea surface temperature anomalies (SSTAs) on interannual and longer time scales. On interannual time scales, a horseshoe-shape structure, characterized by equatorially symmetric SSTAs in the tropics and zonally elongated monopole-like anomalies with the opposite polarity in the central North Pacific, is most dominant in the Pacific SST variability in boreal winter. This SST pattern is associated primarily with the well-known Pacific/North American (PNA) and/or Western Pacific teleconnection patterns in the atmosphere [*Wallace and Gutzler*, 1981], which induce basin-wide changes in the mid-latitude surface westerlies. On decadal time scales, a different pattern has been identified from a careful selection of an analysis domain for modal decomposition of the variability. *Nakamura et al.* [1997a] and *Nakamura and Yamagata* [1999] identified decadal SST variability along the western Pacific subarctic frontal zone (SAFZ) in [36~44^{o}N, 140~180^{o}E], which is simultaneously uncorrelated with tropical SSTAs, as confirmed in a local correlation analysis by *Tomita et al.* [2001]. Since a wave-activity flux of stationary Rossby waves applied to the

associated anomaly patterns of 500-hPa geopotential height is strongly divergent over the SAFZ and pointing equatorward to the south [*Nakamura and Yamagata*, 1999], those atmospheric anomalies are likely to be locally forced and/or maintained rather than associated with the extratropical remote response to the tropical SST forcing.

Since temporal fluctuations of atmospheric teleconnection patterns in the extratropics strongly affect wintertime climatic conditions, atmospheric general circulation model (AGCM) experiments have been carried out to assess the relative importance of tropical and extratropical SSTAs in forcing year-to-year atmospheric variations [e.g., *Lau and Nath*, 1994]. In most of the experiments, distinct remote response was simulated in the North Pacific to the tropical Pacific SSTAs. The response was realized under both perpetual and time-varying SSTA forcing. In contrast, most of the AGCMs failed to generate any systematic response to the local extratropical SSTAs even to the perpetually prescribed SSTAs. These AGCM experiments carried out thus far have led to a general consensus that the tropical (extratropical) upper ocean is an active (a passive) medium to the local atmospheric forcing [see *Kushnir et al.*, 2002].

One of the reasons for the strong model dependence of extratropical atmospheric response to given local SSTAs is the differences in the treatment of planetary boundary layer (PBL) processes among those models. Several experiments in each of which an AGCM is coupled thermally with a one-dimensional ocean mixed layer [e.g., *Lau and Nath*, 1996, 2001; *Watanabe and Kimoto*, 2000] indicated that the extratropical ocean acts to reinforce overlying atmospheric teleconnection patterns induced by tropical SSTAs, modulating their spatial structure and prolonging their intra-seasonal persistence. This weak local feedback from SSTAs to atmospheric anomalies is known as "reduced thermal damping" [*Kushnir et al.,* 2002], as elucidated in a simple, linearized coupled model by *Barsugli and Battisti* [1998].

Very recently, *Xie et al.* [2002] showed that a regional atmospheric model (MM5) with a carefully treated PBL exhibits a clear sensitivity of regional cyclogenesis to the sharpness of local SST gradient in the East China Sea. In addition, the decadal variability confined in the extratropical Pacific as observed is simulated in a coupled general circulation model where air-sea coupling is allowed only in the extratropics [*Liu et al.*, 2002]. These numerical experiments suggest a two-way nature of air-sea interaction in the extratropics, although the aforementioned observational studies have clearly revealed only the atmospheric forcing with no solid evidence for possible, though maybe subtle, feedback from the ocean. Observational detection of the latter feedback thus requires a careful diagnosis of observed data, including those of turbulent heat fluxes.

As well established, the turbulent latent and sensible heat fluxes (upward positive) are determined by in-situ scalar wind speed at the sea surface, temperature and moisture differences, respectively, between that surface and the bottom of PBL, through the so-called aerodynamic bulk formulae as below;

$$Q_E = \rho_a L C_E U_a \left(q_s(T_s) - q_a(T_a)\right)$$
$$\text{and} \qquad (1)$$
$$Q_H = \rho_a c_p C_H U_a (T_s - T_a)$$

In these formulae, Q_E and Q_H are the latent and sensible heat fluxes, respectively, ρ_a is the air density, c_p the specific heat of air at constant pressure, L the latent heat of vaporization for water, U_a the scalar wind speed at 10m above the sea surface, and C_H and C_E are bulk coefficients for

temperature (T) and humidity (q), respectively. Subscripts s and a indicate values measured at the sea surface and 10m aloft, respectively. A change in any of these variables leads to anomalies in Q_E and Q_H. As mentioned earlier, the most dominant mode of basin-scale SST variability is accompanied by large-scale atmospheric circulation anomalies. Associated changes in scalar wind speed, surface air temperature (SAT) and surface air humidity are therefore spatially and temporally coherent to cause large-scale turbulent heat flux variations that force the basin-scale SSTA pattern. Those atmospheric changes thus tend to generate temporal variations of the leading SST mode in a month or two, as clearly shown in many previous observational studies, [e.g., *Davis*, 1976; *Frankignoul*, 1985; *Wallace and Jiang*, 1987; *Iwasaka et al.*, 1987; *Frankignoul and Kestenare*, 2002].

Though most dominant, however, the leading SST mode cannot, of course, explain all the observed interannual variance. Modal decomposition analyses, including empirical orthogonal function (EOF) and singular value decomposition (SVD) analyses, tend to define large-scale anomaly patterns as the leading modes of the variability that, if combined, explain a major fraction of the total variance within an analysis domain. When applied to a basin-scale SSTA field, an EOF or SVD analysis thus extracts the leading mode of SST variability that is always associated with planetary or basin-scale atmospheric anomalies. Since the ocean has a deformation radius inherently much smaller than the atmospheric counterpart, those analysis methods are therefore not particularly suited for extracting physically significant but smaller-scale SSTA patterns induced primarily by oceanic processes.

In addition to the one-dimensional thermal coupling across the sea surface as discussed in *Barsugli and Battisti* [1998] and *Kushnir et al.* [2002], three-dimensional ocean dynamics is also essential in forming SSTAs in such a region as near the SAFZ [*Qiu and Kelly*, 1993; *Qiu*, 2000]. Careful inspections of ocean general circulation model (OGCM) hindcasts, experiments, and assimilated data for several decades have suggested that interannual to decadal SST variations near SAFZ or Kuroshio-Oyashio extension are very much influenced by changes in the ocean conditions in this inter-gyre region [*Xie et al.,* 2000; *Seager, et al.* 2001; *Schneider and Miller*, 2001; *Schneider et al.*, 2002; *Tomita et al.*, 2002]. A steady strong current of the Kuroshio and Oyashio extension advects a large amount of heat into the region, where a dry cold air mass continuously supplied by the East Asian winter monsoon leads to a huge amount of heat loss from the sea surface. Therefore changes in either of these independent processes or both in the ocean and atmosphere regulate the air-sea temperature difference. Specifically, SSTAs formed through ocean dynamics can act to change the turbulent heat fluxes above the sea surface, while anomalies in marine meteorological variables (U_a, q_a and SAT) can act to modify those SSTAs by altering the fluxes. Most of the previous statistical studies have presented evidence that the atmospheric variables are primarily responsible for determining turbulent heat fluxes. In fact, generally over the extratropical North Pacific, SSTAs are negatively correlated with local anomalous upward turbulent heat fluxes, indicative of the predominance of the atmospheric forcing upon the SSTAs [e.g., *Hanawa et al.*, 1995]. A closer look of Figure 6a of *Hanawa et al.* [1995], however, reveals positive SST-flux correlation hinted in the westerly boundary current region. Although the spatial resolution of the data is too sparse to solidly identify the positive correlation as a physically meaningful signal, this positive correlation suggests a potential that SSTAs in that particular extratropical region can force the overlying atmosphere like in the tropics.

A conventional cross-correlation analysis can show a local relationship between SSTAs and anomalous turbulent heat fluxes, but it does not tell us which variable is the most deterministic. To diagnose relative importance among anomalies in SST, q_a, SAT, and U_a in determining latent and sensible heat flux anomalies at a given instance, we linearized the formulae (1) and thereby decomposed the total amount of turbulent heat fluxes into three components, following *Halliwell and Mayer* [1996] as described in Section 2. In that way, we will see whether or not extratropical SSTAs on the interannual and decadal time scales can play an active role in determining local turbulent heat fluxes, based on the observational archives.

The rest of paper is organized as follows. Section 2 describes a new data set of linearized turbulent heat fluxes constructed for the present study. Section 3 shows the local cross-correlation between SSTAs and other meteorological variables such as the scalar wind speed and surface air temperature anomalies (SATAs). Section 4 presents total and linearized heat flux anomalies associated with the dominant patterns of SST variations. Section 5 discusses a reliability of our results after a summary is given.

2. A linearized turbulent heat flux data set

A data set of marine meteorological variables with 2^o longitude-latitude resolution has been constructed for the North Pacific from quality-controlled ship and buoy observations compiled in the Long Marine Reports in fixed length record (LMRF) of the so-called Comprehensive Ocean-Atmosphere Data Set [COADS; *Woodruff et al.*, 1987]. Fields of SST, humidity, SAT, vector and scalar surface wind were used in constructing fields of latent and sensible heat fluxes. The fluxes have been calculated on the basis of *Kondo*'s [1975] aerodynamic bulk method. Details of the calculation are described in *Tanimoto et al*. [1997] and *Tanimoto and Xie* [2002]. Although 10-day mean fields were originally prepared, flux anomaly fields averaged over two or three winter months are used in this analysis.

As explained in Introduction, latent and sensible heat fluxes inherently depend on SST, q_a, SAT, and U_a. We linearized each of those fluxes, to assess which is the most dominant factor in determining the sign of a flux anomaly. By dividing each of the variables into the climatological mean and the deviation from it, each of the fluxes can be expressed as a sum of the contributions from the climatological mean and anomalies; i.e.,

$$\begin{aligned} Q_E &= \rho_a L C_E U_a (q_s - q_a) \\ &= \rho_a L C_E (\overline{U_a} + U_a{}') \\ &\bullet \left\{ (\overline{q_s}(\overline{T}_s) + q_s'(T_s')) - (\overline{q_a}(\overline{T}_a) + q_a'(T_a')) \right\} \end{aligned} \tag{2}$$

and

$$\begin{aligned} Q_H &= \rho_a c_p C_H U_a (T_s - T_a) \\ &= \rho_a c_p C_H (\overline{U_a} + U_a{}') \\ &\bullet \left\{ (\overline{T_s} + T_s') - (\overline{T_a} + T_a') \right\} \end{aligned} \tag{3}$$

The climatological-mean heat flux is given as the sum of a contribution from the climatological means of the individual variables and a much smaller contribution from their anomalies; i.e.,

$$\overline{Q_E} = \rho_a L C_E \left\{ \overline{U_a}(\overline{q_s} - \overline{q_a}) + \overline{U_a^{'}(q_s^{'} - q_a^{'})} \right\} \qquad (4)$$

and

$$\overline{Q_H} = \rho_a c_p C_H \left\{ \overline{U_a}(\overline{T_s} - \overline{T_a}) + \overline{U_a^{'}(T_s^{'} - T_a^{'})} \right\} \qquad (5)$$

Thus, the anomalous fluxes at a particular instance at a given location can be expressed as follows:

$$\begin{aligned} Q_E^{'} &= Q_E - \overline{Q_E} \\ &= \rho_a L C_E \left\{ \overline{U_a} q_s^{'} - \overline{U_a} q_a^{'} + U_a^{'}(\overline{q_s} - \overline{q_a}) \right. \\ &\quad \left. + \left[U_a^{'}(q_s^{'} - q_a^{'}) - \overline{U_a^{'}(q_s^{'} - q_a^{'})} \right] \right\} \end{aligned} \qquad (6)$$

and

$$\begin{aligned} Q_H^{'} &= Q_H - \overline{Q_H} \\ &= \rho_a c_p C_H \left\{ \overline{U_a} T_s^{'} - \overline{U_a} T_a^{'} + U_a^{'}(\overline{T_s} - \overline{T_a}) \right. \\ &\quad \left. + \left[U_a^{'}(T_s^{'} - T_a^{'}) - \overline{U_a^{'}(T_s^{'} - T_a^{'})} \right] \right\} \end{aligned} \qquad (7)$$

We focus on the first three terms of the right hand side of (6) and (7) in the following analysis since the last two terms have indeed been found negligible. The first three terms of (7) are considered to represent the respective contributions from SSTA, SATA and $U_a^{'}$, in this order, to the total sensible heat flux anomaly. This linearization does not necessary mean that these three variables are always independent of each other. To avoid any complication in the following section, we will use the same terminology for the corresponding individual contributions of (6) to the anomalous latent heat flux because surface humidity anomalies strongly depend on local SATAs. This is reasonable in the light of good correlation generally observed between SATAs and surface humidity anomalies [*Kleeman and Power,* 1995]. We should note that the bulk coefficients in Kondo's formulae also depend on the air-sea temperature difference and scalar wind speed. For simplifying interpretation of our analysis, however, any contribution from that particular dependency to the linearized components is ignored in the present study.

Neither spatial smoothing nor filtering for obtaining better-looking pictures was imposed on the flux fields. As explained in the Introduction, this study aims to identify a rather subtle signal in the extratropical air-sea interaction whose spatial scale may be much smaller than that of the basin. In particular, at least 2^{o} resolution is required for a careful analysis of the frontal regions. We take the advantage of avoiding data distortion, despite relatively large sampling errors that may be included in those unsmoothed maps with relatively high spatial resolution, even averaged over the entire winter season.

3. Local cross-correlation analysis

Figure 1c shows a map of local correlation coefficients over the North Pacific between the January-February-March (JFM) mean SSTAs and the December-January-February (DJF) mean combined latent and sensible heat flux anomaly. In Figures 1a and 1b, the same SSTAs are locally correlated with the individual contributions of $U_a^{'}$ and SATAs, respectively, to that flux anomaly. The lead-lag relationship between the SSTAs and each of the other three variables is reversed in Figure 2. When anomalies in U_a lead to local SSTAs, their correlation is strongly negative particularly over the central basin (Figure 1a). The region of the strongest negative corre-

Figure 1

Figure 2

lation (stronger than -0.6) corresponds to the center of action of the dominant SST variability [*Nitta and Yamada*, 1989; *Tanimoto et al.*, 1997; *Zhang et al.*, 1997]. This spatially coherent structure reflects the strengthening (weakening) of the surface westerlies that enhances (suppresses) local evaporative cooling, in cooperation with additional contributions from enhancement (suppression) of both southward Ekman transport and mechanical vertical mixing. The apparent tendency that their correlation becomes weaker and spatially less coherent when SSTA is taken as the lead variable (Figure 2a) is consistent with the primary role of the surface westerlies in generating SSTAs.

In both of the lead and lag correlations, the local SATA contribution to the flux anomalies, which is negatively proportional to the SATA itself, is negatively correlated with local SSTAs over most of the domain (Figures 1b and 2b). The region of the strongest negative correlation in each of their correlations almost coincides with the region of the strongest negative correlation in Figure 1a. This strong negative correlation between DJF mean SATA contribution and JFM SSTAs indicates that the enhanced (reduced) coolness of the maritime air associated with the strong (weak) westerlies under the climatological-mean eastward SAT gradient also contributes to the enhanced (suppressed) evaporation, as supported by the significant negative correlation of $U_a^{'}$ and SATAs over the central basin (Figure 3). In fact, the correlation between total linearized flux anomalies and the SSTAs is negative over the central basin (Figure 1c), reflecting the prevailing atmospheric forcing on SSTAs through $U_a^{'}$ and SATAs. However, even when SSTAs are taken as the lead variable (Figure 2b), negative correlation is still significant around the center of action. This tendency indicates a two-way air-sea interaction at the sea surface, where SATAs may be adjusted toward a thermally more equilibriated state with the underlying SSTAs that have been already generated by the predominant atmospheric forcing.

Figure 3

It is noteworthy that the negative correlation between $U_a^{'}$ and SSTA is very weak or their correlation is even weakly positive in the coastal regions of the basin and over the western North Pacific (Figures 1a and 2a), which is consistent with a recent study by *Nonaka and Xie* [2003]. Enhanced vertical mixing in the atmospheric boundary layer over warm SSTAs may contribute to positive correlation coefficients between SSTA and $U_a^{'}$ [*Xie et al*. 2002, *Nonaka and Xie*, 2003]. This positive correlation is indicative of an active role of SSTAs in air-sea interaction over those regions. In fact, when the sum of all the linearized components of the flux leads SSTAs, their correlation is positive along the SAFZ in [35~45^{o}, 140~165^{o}E] indicated by the inset rectangle of Figure 1c, in which no spatially coherent correlation structure is observed between the atmospheric contributions to the flux and SSTAs (Figures 1a and 1b). This positive correlation along the SAFZ suggests that a contribution of SSTA to local heat flux anomalies dominates over a counteracting contribution from the atmospheric anomalies. In fact, when we take the SSTAs as the lead variable, positive correlation becomes even more significant and spatially coherent along the SAFZ (Figure 2c). Even in some other parts of the basin, the correlation turns into weakly positive. This tendency of the correlation between SSTA and total turbulent heat flux supports the notion of the two-way air-sea interaction at the sea surface in the extratropics. The tendency also suggests the dominant role of oceanic influence in determining the local turbulent heat flux anomalies over the coastal region and SAFZ. In the next section, we will assess the relative importance of individual components of the linearized turbulent heat flux anomalies observed in association with the dominant SSTA structures

over the central basin and along SAFZ, separately. This separate treatment of these two regions is suggested by previous modal decomposition analyses through which the loadings of the two leading modes have been found to be fairly well separated, one over the central basin and the other in and along SAFZ, respectively [*Kawamura*, 1994; *Deser and Blackmon*, 1995; *Tanimoto et al.*, 1997; *Nakamura et al.*, 1997a].

4. Composite analysis

Figure 4 presents two types of spatial structures dominant in interannual SST variability in the North Pacific. *Nakamura et al.* [1997a] and *Nakamura and Yamagata* [1999] presented that SST time series at several different locations around SAFZ exhibit pronounced decadal fluctuations that are uncorrelated with the tropical SST variability. To represent the warm and cold phases of this wintertime decadal variability in the SAFZ, we selected a pair of 4-year periods; 1968/69-71/72 winters (category DC+) and 1982/83-1985/86 winters (category DC-), based on Figure 3a in *Nakamura et al.* In the middle upper panel (Figure 4b) for the January-February period, significant positive SSTAs over 1.0 ^{o}C are confined in the narrow zonal band [36~44^{o}N] in the western half of the domain, indicating SAFZ fluctuations. From the early winter (November-December; Figure 4a) to late winter (March-April; Figure 4c), the SSTAs near SAFZ extend to the east while broadening meridionally with the development of secondary maxima centered at [30^{o}N, 160^{o}W] by the March-April period. Note that negative anomalies localized at two particular grid points [40^{o}N, 175^{o}W] and [40^{o}N, 165^{o}W] are less reliable due to erroneous ship reports included in the original COADS LMRF archives [*Minobe*, 2002, personal communication].

Figure 4

A time-scale separation method applied to the North Pacific SSTA field has revealed that fluctuations with interannual and decadal time scales are found comparable in amplitude over the North Pacific [*Tanimoto et al.*, 1997; *Zhang et al*., 1997; *Nakamura and Yamagata,* 1999; *Nakamura and Kazmin,* 2002]. The former fluctuations in the central basin are associated primarily with the El Niño-Southern Oscillation (ENSO). On the basis of Table 3 in *Tanimoto et al.*, we chose 1967/68, 70/71, 73/74, 84/85 winters (category IA+) and 1969/70, 72/73, 82/83, 87/88 winters (category IA-) as the particularly warm and cold winters, respectively, with respect to interannual SSTAs in the central basin. Three out of four winters in the category IA+ and all the four winters in the category IA- thus correspond to the cold and warm phases of ENSO, respectively. In the midwinter interannual composite (Figure 4e), positive SSTAs over 1.0 ^{o}C spread more widely in the latitudinal direction over the central basin than in its decadal counterpart (Figure 4b), while negative SSTAs are found west of 160^{o}E to the south of Japan.

4.1. Decadal scales (categories DC+ and DC-)

Composite difference maps between the categories DC+ and DC- have been constructed for surface wind velocity (Figure 5) and the linearized latent heat flux including its individual components (Figure 6). Those maps were constructed separately for the December-January and February-March periods. These bi-monthly periods have been selected in such a way that the anomalous heat flux forcing corresponds to the tendency of bi-monthly SSTAs in Figure 4. These maps correspond to the warm phase of SAFZ associated with the decadal variability. The sign of each of the flux anomalies should be reversed when discussing the cold phase. We should note here that the positive (negative) heat flux anoma-

Figure 5

Figure 6

lies mean enhanced (suppressed) heat release for the ocean surface, thus represented with blue and purple (orange and red) colors in these figures. This coloring is thus counterintuitive from the viewpoint of the atmospheric thermal forcing.

During the December-January period, surface wind anomalies (Figure 5a) are anticyclonic mostly over the basin, accompanied by the weakening of the surface westerlies in the central basin [20~40^{o}N, 150^{o}E~150^{o}W]. A northerly monsoonal flow also weakens south of Japan and over the East China Sea, whereas the monsoonal northwesterlies prevailing to the north undergo no substantial changes. Off the west coast of North America, northwesterly wind anomalies weaken the warm air advection from the south, acting to form negative SSTAs along the coast (Figures 4b and 4c), in cooperation with the additional cooling via induced anomalous coastal upwelling. The aforementioned atmospheric forcing associated with the anticyclonic wind anomalies acts to expand the existing warm SSTAs eastward and southward in the central part of the basin, while generating cool SSTAs along the west coast of North America, which accounts for the seasonal evolution of the observed SSTAs. Though weakened, the anticyclonic wind anomalies still remain to the south of the Aleutian Islands during the February-March period, reinforcing SSTAs that have been generated by midwinter.

Reflecting those atmospheric anomalies that are incorporated in the individual components of the turbulent heat flux, the total latent heat flux anomalies shown in Figure 6a display a southwest-northeast tilted band of suppressed heat release extending from [20^{o}N, 120^{o}E] all the way to [40^{o}N, 160^{o}W]. The resultant surface warming generated in this tilted band during the December-January period is in good correspondence to the warming SST tendency observed in the same region (Figures 4a and 4b). A half degree temperature increase in a mixed layer of 125m depth is nearly equivalent to 50 Wm^{-2} of total (latent plus sensible) surface heat flux anomalies imposed over two months, which is consistent with the SSTA changes along that tilted band as represented in the composite maps. The effect of the weakened westerlies (Figures 6g and 5a) and positive SATAs (Figure 6e) associated with the anticyclonic anomalies are major contributors to the surface warming, dominating over the compensating effect of the positive SSTAs (Figure 6c). It can be thus interpreted that the observed warming within the particular band is forced by the atmospheric anomalies, and so is the cooling tendency observed off the west coast of North America.

The situation, however, seems the opposite in the SAFZ (Figures 6c and 6d), where SSTAs are positive (Figures 4a-c) and so are correlation coefficients between SSTAs and upward turbulent heat flux anomalies (Figures 1c and 2c). In a small region off the east coast of Japan at ~40^{o}N indicated by the inset rectangle of Figure 6a, turbulent latent heat flux anomalies are anomalously upward, acting to yield the surface cooling in the warm SAFZ during the December-January period. In this region where SSTAs and anomalous turbulent heat fluxes are positively correlated in the rectangles in Figures 1c and 2c, the effect of SATAs is toward the SST warming (Figure 6e), whereas $U_A^{'}$ is not strong enough to make any significant contribution to the anomalous heat flux (Figure 6g). It is the warm SSTAs that dominantly contribute to the SST cooling (Figure 6c). In other words, the observed SSTAs act to force the lower troposphere, while damping themselves through the enhanced heat release into the atmosphere. It is noteworthy that the contributions from SSTAs (Figure 6c) and SATAs (Figure 6e), which normally tend to compensate one another, exhibit different meridional scales in the western Pacific, perhaps reflecting different deformation radii between atmospheric and oceanic flows. Since SSTAs

are significantly positive only along the narrow SAFZ, this is the only region where the SSTA contribution to the total latent heat flux anomalies dominates over the counteracting contributions from the atmospheric anomalies. As the atmospheric anticyclonic anomalies gradually weaken by late winter and early spring (Figure 5b), the atmospheric contribution to the anomalous heat flux reduces (Figures 6f and 6h), leading to the increasing role of the SSTA contribution (Figure 6d). As a consequence, surface cooling along the warm SAFZ becomes even stronger in late winter, extending its zonal extent (Figure 6b). The weakening of the atmospheric anticyclonic anomalies, in turn, implies that the SSTA forcing on the atmosphere, if exists, would be rather modest. Though considerably weaker, the anomalous sensible heat flux is distributed spatially in a manner very similar to that of the anomalous latent heat flux (not shown).

4.2. Interannual time scales (categories IA+ and IA-)

Figure 7 shows composite difference maps of the surface wind velocity and its speed between the categories IA+ and IA-. The most striking feature for the December-January period is a northwest-southeast tilted band of the weakened westerlies, extending central and eastern portions of the basin (Figure 7a). To the south, surface wind speed tends to be stronger by up to 1m s^{-1} than its climatological mean, although the anomalous wind velocity exhibits no coherent pattern in the same area. Wind speed also tends to be weaker off the west coast of North America, despite the fact that the alongshore wind component is in the same sense as in the case shown in Figure 5. Since the alongshore component is perpendicular to the climatological southwesterlies, the anomalous wind speed depends sensitively on the amplitude of the anomalous surface wind velocity. These surface wind anomalies shown in Figure 7a are associated with distinct anticyclonic anomalies over the basin, as a remote response to the tropical SSTAs as in La Niña winters. Sign of each of the anomalies should be reversed in discussing the situation for El Niño winters.

In a difference composite map of the total latent heat flux for the same early winter season (Figure 8a), suppressed heat release prevails over that tilted region of the reduced wind speed, and the enhanced heat release to its southwest. The anomalous wind speed contributes only a little, though positively, to the observed surface flux forcing (Figure 8g). Rather, SATAs are the major contributor to the anomalous heat flux (Figure 8e). The spatial correspondence between the SATA contribution and the anomalous heat flux is good over the entire basin, except off Baja California, where the SSTA determines the heat flux anomaly (Figures 8a and 8c). The reasonably good correspondence between the SATA contribution (Figure 8e) and observed SST evolution into midwinter (Figures 4d and 4e) suggests the prevailing atmospheric forcing via SATA on the seasonal evolution of the observed SSTA, which overcomes the counteracting effect from SSTAs, as indicated in the previous studies.

A difference composite map in Figure 7b indicates that the wind speed anomaly pattern undergoes a marked change by the February-March period. The midlatitude region of the weakened surface westerlies becomes more zonally oriented, extending entirely across the basin. A striking feature found in the latent heat flux anomalies is the suppressed heat release that occurs off the east coast of Japan and farther to the east (Figure 8b). To the east of 150°E, both the positive SATAs and reduced wind speed (Figures 8f and 8h) contribute to this suppression (Figure 8b). Presumably, the weakened westerlies act to reduce the supply of a cold and dry air mass from the Eurasian continent, which apparently contributes to the main-

Figure 7

Figure 8

tenance of the local positive SSTAs. Just off the southern coast of Japan, in contrast, SATAs have been negative since early winter (Figures 8e and 8f), despite the slight weakening of the East Asian winter monsoon (Figure 7). The suppressed latent heat release observed just south of Japan is found due primarily to the negative SSTAs in that region (Figure 8d), indicative of oceanic forcing on the overlying atmosphere. Essentially the same characteristics as mentioned above are found in the anomalous sensible heat flux field (not shown).

5. Concluding remarks

We have examined the spatial structures of anomalous turbulent heat fluxes at the sea surface associated with the dominant SSTA patterns in the North Pacific, by utilizing a carefully constructed data set with relatively higher resolution (2^o longitude-latitude) than currently available data sets on the basis of in-situ ship measurements. Our correlation analysis has revealed a dual role of the turbulent heat flux anomalies in extratropical air-sea interaction. In the central North Pacific, the local SSTA and SATA contributions to the turbulent heat flux anomalies are negatively correlated under very weak influence of continental air masses (Figures 1b and 2b). These negative lead-lag correlation coefficients indicate that these two contributions are not completely independent. The thermal adjustment occurs at the sea surface in this portion of the basin, leading to the mutual compensation between SSTA and SATA contributions. (Figures 6 and 8).

As argued in *Xie and Seki* [1997], however, air-sea differences in temperature and specific humidity are not always constant. The SSTA and SATA contributions to the local turbulent heat flux anomalies are not well correlated near the SAFZ and Kuroshio extension regions. These contributions to the flux anomalies have different spatial scales to one another in the composite maps (Figures 6 and 8). These findings indicate that these contributions are determined by different processes. Hence it is meaningful to separate individual contributions, especially in the SAFZ and coastal regions. In the present study, linearization of the anomalous turbulent heat flux applied to a given phase of the dominant SST variability has further elucidated the counteracting contributions from the atmospheric and SST anomalies to the local heat flux anomalies. In the central and eastern portions of the basin, where the wind anomalies are relatively strong, the atmospheric contribution to the total turbulent heat flux anomalies dominates over the SSTA contribution on both decadal and interannual time scales. In these regions, atmospheric anomalies thus locally force SSTA by changing the heat flux, in good agreement with a number of previous studies.

However, in such regions as the narrow SAFZ and the region south of Japan, SSTAs on decadal and interannual time scales determine the sign of local heat flux anomalies and thereby act to force the overlying atmosphere thermally. In those regions where anomalies in the surface wind speed tend to be relatively weak, the advective effect of the Kuroshio and/or Oyashio currents estimated with satellite altimeters probably dominates in determining local SSTAs over the direct thermal forcing from the atmosphere [*Qiu and Kelly*, 1993; *Qiu*, 2002]. The primary importance of oceanic processes in forming SSTAs near SAFZ has been already suggested by OGCM simulations [*Xie et al.*, 2000; *Seager et al.*, 2001; *Schneider and Miller*, 2001; *Schneider et al.,* 2002] and by model-assimilated data [*Tomita et al.*, 2002]. Our composite analysis has shown that SSTAs confined in the SAFZ, which characterize the decadal-scale variability in the North Pacific [*Nakamura et al.*, 1997a], act to force the atmosphere thermally, as suggested in a coupled GCM study by *Schneider*

et al. [2002]. There, as SST increases, the more heat is released into the atmosphere via turbulent fluxes from the ocean surface, just like in the tropics. This active role of those decadal SSTAs we have revealed in the air-sea heat exchange within the SAFZ is apparently beyond the effect of reduced thermal damping [*Barsugli and Battisti,* 1998].

Whether or not the early-winter pattern of atmospheric circulation anomalies shown in Figure 5a is indeed generated in response to the pre-existing SSTAs in the SAFZ (Figure 4a), it has been shown in our analysis that those atmospheric anomalies force SSTAs with the opposite sign from mid- to late winter over the Gulf of Alaska, so as to form a see-saw-like relationship observed between the two regions as a characteristic feature of the decadal SSTA pattern inherent in the extratropical North Pacific [*Nakamura et al.*, 1997a]. The atmospheric anomalies also act to extend the pre-existing SSTAs in the SAFZ into the eastern portion of the basin by late winter. It is therefore possible that two-way atmosphere-ocean interaction via anomalous turbulent heat flux over the extratropical North Pacific can account for the observed seasonal evolution of SSTAs and atmospheric anomalies associated with the decadal climate variability. Essentially the same kind of SSTA forcing as above on the atmosphere has been found in the Kuroshio region south of Japan as a part of the ENSO-associated anomalies, although the spatial structure of those SSTAs is very different from that in the decadal time scales.

Accompanied by the decadal-scale SSTAs in the SAFZ (Figures 4a-c), stationary anticyclonic anomalies are observed over the central part of the basin from the surface (Figure 5) up to the 250-hPa level (Figure 9). A wave-activity flux developed by *Takaya and Nakamura* [2001] strongly diverges out of this upper-level PNA-like anticyclonic anomalies (Figure 9a), which is consistent with a similar diagnosis by *Nakamura and Yamagata* [1999] applied to the 500-hPa level. The results suggest that the PNA-like stationary anomalies are locally forced in association with the decadal-scale SSTAs in the SAFZ. Although the specifics of the forcing are unknown at this stage, one possible mechanism may be the involvement of a nearby storm track, as already suggested by recent AGCM experiments [*Peng and Whitaker*, 1999; *Watanabe and Kimoto*, 2000; *Kushnir et al.*, 2002]. As shown in Figures 6c and 6d, the SSTA contribution dominates over the counteracting atmospheric contributions only around the SAFZ located slightly north of the Kuroshio axis and its downstream extension. In the presence of warm SSTAs in the SAFZ the associated local enhancement of heat release into the atmosphere acts to augment the meridional thermal contrast near the surface along the northern flank of the SAFZ while relaxing the contrast along the Kuroshio axis. The combined effect would lead to the slight northward shift of a near-surface baroclinic zone over the western Pacific. Likewise, the baroclinic zone would be slightly shifted southward in the presence of decadal-scale cool SSTAs in the SAFZ. In fact, *Nakamura and Kazmin* [2002] observed such decadal modulations in the cross-frontal thermal contrast in the SAFZ. During early winter when westerlies are modestly strong, the storm track activity over the North Pacific is positively correlated with the low-level baroclinicity [*Nakamura*, 1992]. One would therefore imagine that the Pacific storm track (i.e., the zonal band of high activity of atmospheric baroclinic disturbances) would shift northward, in the presence of warm SSTAs in SAFZ as in Figure 4a that act to shift the baroclinic zone northward. Figure 9b indicates that is really the case. In this figure, the storm track activity is measured by the anomalous poleward heat flux at the 850-hPa level associated with subweekly disturbances [*Nakamura et al.*, 2002], on the

Figure 9

basis of the NCEP/NCAR reanalysis data set. The northward shift of the storm track activity results in the reduction in the poleward vorticity transport by upper-tropospheric eddies at ~35°N. The 250-hPa geopotential height tendency due solely to the anomalous eddy vorticity flux convergence [*Nakamura et al.*, 1997b] exhibits the anticyclonic forcing over the central part of the basin, reinforcing the existing stationary anticyclonic anomalies (Figure 9c). Thus the oceanic thermal forcing might indirectly reinforce atmospheric circulation anomalies through winter.

Our successful identification of the oceanic thermal forcing upon the atmosphere in a midlatitude frontal zone is owing to the characteristics of our data set and analysis methods. Unlike in most of the previous studies, we utilized a data set whose spatial resolution exceeds the minimal for resolving meridionally narrow frontal zones. We avoided applying any basin-wide modal decomposition (EOF or SVD) analysis or any spatial smoothing. Our usage of carefully analyzed in-situ ship observation data was also critical for our successful analysis. To ensure the fidelity of our observational results, latent and sensible heat flux data in the NCEP/NCAR reanalyses are also analyzed. In latent heat flux anomalies in the reanalysis data (Figure 10), signature of such oceanic forcing on the atmosphere as identified in our COADS data set is actually hinted, but the signature is substantially weaker (cf., Figures 6a and 6b) despite the comparable spatial resolutions between the two data sets. Recent re-evaluation studies of the turbulent heat fluxes for the Atlantic [*Sun et al.*, 2003] and for the western boundary current regions [*Moore et al.*, 2002] have revealed that excessively large values of the roughness length for the bulk formulae were used in the reanalyses in evaluating turbulent heat fluxes under high-wind situations. Overestimation in the latent heat flux of reanalyses is also reported in comparisons with in-situ observations in Labrador sea [*Renfrew et al*. 2002] and those made during WOCE [*Smith et al*. 2001]. It is therefore likely that the atmospheric contribution is overestimated in the surface heat fluxes of the NCEP/NCAR and ECMWF reanalyses, which probably masks the oceanic contribution. Rederiving the fluxes using surface marine meteorological variables from the reanalyses and TOGA-COARE flux algorithm was successful to reduce the overestimation **[***Moore et al.*, 2002; *Sun et al.*, 2003]. An overall reevaluation of the turbulent fluxes in reanalysis data sets is desired for the world ocean.

Acknowledgments. The authors are grateful to Profs. S.-P Xie and S. Minobe for stimulating discussions. They are also grateful to Drs. N. Iwasaka, R. Zhang, and M. Honda for their preparing the data sets used in the present study. A number of valuable comments given by two referees and a useful comment by the Editor (Dr. J. Toole) are appreciated. This work is under the support of the Frontier Research System for Global Change sponsored by Japan Marine Science and Technology Center.

Figure 10

References

Barsugli, J.J., and D.S. Battisti, The basic effects of atmosphere-ocean thermal coupling on midlatitude variability, *J. Atmos. Sci*., *55*, 477-493, 1998.

Davis, R.E., Predictability of sea surface temperature and sea level pressure anomalies over the North Pacific Ocean, *J. Phys. Oceanogr.*, *6*, 249-266, 1976.

Deser, C., and M.L. Blackmon, On the relationship between tropical and North Pacific sea-surface temperature-variations, *J. Clim., 8*, 1677-1680, 1995.

Frankignoul, C., Sea surface temperature anomalies, planetary waves and air-sea feedback in the middle latitudes, *Rev. Geophys.*, *23*, 357-390, 1985.

Frankignoul, C., and E. Kestenare, The surface heat flux feedback. Part I: estimates from observations in the Atlantic and the North Pacific, *Clim. Dyn.*, *19*, 633-647, 2002.

Halliwell, G.R., and D.A. Mayer, Frequency response properties of forced climatic SST anomaly variability in the North Atlantic, *J. Clim., 9*, 3575-3587, 1996.

Hanawa, K., R. Sannomiya and Y. Tanimoto, Static relationship between anomalies of SSTs and air-sea heat fluxes in the North Pacific, *J. Meteoro. Soc. Japan, 73*, 757-763, 1995.

Iwasaka, N., K. Hanawa, and Y. Toba, Analysis of SST anomalies in the North Pacific and their relation to 500mb height anomalies over the Northern Hemisphere, *J. Meteoro. Soc. Japan, 65*, 103-114, 1987.

Kawamura, R., A rotated EOF analysis of global sea surface temperature variability with interannual and interdecadal scales, *J. Phys. Oceanogr., 24,* 707-720, 1994.

Kleeman, R., and S.B. Power, A simple atmospheric model of surface heat flux for use in ocean modeling studies, *J. Phys. Oceanogr.*, *25*, 92-105, 1995.

Kondo, J., Air-sea bulk transfer coefficient in diabatic conditions, *Bound -Layer Meteor., 9*, 91-112, 1975.

Kushnir, Y., W.A. Robinson, I. Blade, N.M.J. Hall, S. Peng and R. Sutton, Atmospheric GCM response to extratropical SST anomalies: synthesis and evaluation, *J. Clim*., 2233-2256, 2002.

Lau, N.-C., and M.J. Nath, , 1994: A modeling study of the relative roles of tropical and extratropical SST anomalies in the variability of the global atmosphere-ocean system, *J. Clim., 7*, 1184-1207, 1994.

Lau, N.-C., and M.J. Nath, The role of the "atmospheric bridge" in linking tropical Pacific ENSO events to extratropical SST anomalies, *J. Climate, 9*, 2036-2057, 1996.

Lau, N.-C., and M.J. Nath, Impact of ENSO on SST variability in the North Pacific and North Atlantic: Seasonal dependence and role of extratropical sea-air coupling, *J. Clim., 14*, 2846-2866, 2001

Liu, Z., L. Wu, R. Gallimore, and R. Jacob, Search for the origins of Pacific decadal climate variability. *Geophys. Res. Lett.*, *29* (10), doi:10.1029/ 2001GL013735, 2002.

Moore, G.W.K., and I.A. Renfrew, An assessment of the surface turbulent heat fluxes from the NCEP/NCAR reanalysis over the western boundary currents, *J. Clim., 15*, 2020-2037, 2002

Nakamura, H., Midwinter suppression of baroclinic wave activity in the Pacific, *J. Atmos. Sci.*, *49*, 1629-1641, 1992.

Nakamura, H., G. Lin, and T. Yamagata, Decadal climate variability in the North Pacific during the recent decades, *Bull. Amer. Meteor. Soc., 78*, 2215-2225, 1997a.

Nakamura, H., M. Nakamura, and J.L Anderson, The role of high- and low-frequency dynamics in blocking formation, *Mon. Wea. Rev.,125,* 2074-2093, 1997b.

Nakamura, H., and T. Yamagata, Recent decadal SST variability in the Northwestern Pacific and associated with atmospheric anomalies, in *Beyond El Niño: Decadal and Interdecadal Climate Variability*, edited by A. Navarra, pp. 49-72, Springer-Verlag, Berlin 1999.

Nakamura, H., T. Izumi and T. Sampe, Interannual and decadal modulations recently observed in the Pacific storm track activity and east Asian winter monsoon, *J. Clim., 15*, 1855-1874, 2002.

Nakamura, H., and A.S. Kazmin, Decadal changes in the North Pacific oceanic frontal zones as revealed in ship and satellite observations, *J. Geophys. Res., 107,* doi:10.1029/1999JC000085, 2003.

Nitta, T., and S. Yamada, Recent warming of tropical sea surface temperature and its relationship to the northern hemisphere circulation, *J. Meteor. Soc. Japan*, 67, 375-383, 1989.

Nonaka, M., and S.-P. Xie, Co-variations of sea surface temperature and wind over the Kuroshio and its extension: Evidence for ocean-to-atmospheric feedback. *J. Clim.*, in press, 2003.

Peng, S., and J.S. Whitaker, Mechanisms determining the atmospheric response to midlatitude SST anomalies, *J. Clim., 12*, 1393-1408, 1999.

Qiu, B., and K.A. Kelly, Upper-ocean heat balance in the Kuroshio extension region, *J. Phys. Oceanogr., 23*, 2027-2041, 1993

Qiu, B., Interannual variability of the Kuroshio Extension system and its impact on their wintertime SST field, *J. Phys. Oceanogr., 30*, 1486-1502, 2000.

Qiu, B., The Kuroshio extension system: Its large-scale variability and role in the midlatitude ocean-atmosphere interaction, *J. Oceanogr.*, *58*, 57-75, 2002.

Renfrew, I.A., and G.W.K. Moore, P.S. Guest, and K. Bumke, A comparison of surface layer and surface turbulent flux observations over the Labrador Sea with ECMWF analyses and NCEP reanalyses, *J. Phys. Oceanogr, 32*, 383–400, 2002.

Schneider, N., A.J. Miller, Predicting western North Pacific ocean climate, *J. Clim., 14*, 3997-4002, 2001.

Schneider, N., A.J. Miller, D.W. Pierce, Anatomy of North Pacific decadal variability, *J. Clim.*, *15*, 586-605, 2002.

Seager, R., Y. Kushnir, N.H. Naik, M.A. Cane, J. Miller, Wind-driven shifts in the latitude of the Kuroshio-Oyashio extension and generation of SST anomalies on decadal timescales, *J. Clim., 14*, 4249-4265, 2001.

Smith, S.R., D.M. Legler, and K.V. Verzone, Quantifying uncertainties in NCEP reanalyses using high-quality research vessel observations, *J. Clim., 14*, 4062–4072, 2001.

Sun, B., L. Yu, and R.A. Weller, Comparisons of surface meteorology and turbulent heat fluxes over the Atlantic: NWP model analyses versus moored buoy observations, *J. Clim., 16,* 679-695, 2003.

Takaya, K., and H. Nakamura, A formulation of a phase-independent wave-activity flux for stationary and migratory quasigeostrophic eddies on a zonally varying basic flow, *J. Atmos. Sci., 58*, 608-627, 2001.

Tanimoto, Y., N. Iwasaka and K. Hanawa, Relationship between sea surface temperature, the atmospheric circulation and air-sea fluxes on multiple time scales, *J. Meteor. Soc. Japan, 75*, 831-849, 1997.

Tanimoto, Y., and S.-P. Xie, Inter-hemispheric decadal variations in SST, surface wind, heat flux and cloud cover over the Atlantic Ocean, *J. Meteor. Soc. Japan, 79*, 1199-1219, 2002.

Tomita, T., B. Wang, T. Yasunari, and H. Nakamura, Global patterns of decadal-scale variability observed in sea surface temperature and lower-tropospheric circulation fields, *J. Geophys. Res.*, *106*, 26805-26815, 2001.

Tomita, T., S.-P. Xie, and M. Nonaka, Estimates of surface and subsurface forcing for decadal sea surface temperature variability in the mid-latitude North Pacific, *J. Meteor. Soc. Japan, 79*, 1289-1300, 2002.

Wallace, J.M., and D.S. Gutzlar, Teleconnections in the geopotential height field during the Northern Hemisphere winter, *Mon. Wea. Rev.*, *109*, 784-812, 1981.

Wallace, J.M., and Q.-R. Jiang, On the observed structure of the interannual variability of the atmosphere/ocean climate system, in *Atmospheric and Oceanic Variability*, edited by H. Cattle, pp. 17-43, Royal. Meteorological Society, London, 1987.

Watanabe, M., and M. Kimoto, Atmosphere-ocean thermal coupling in the North Atlantic: A positive feedback, *Quart. J. Roy. Met. Soc., 126*, 3343-3369, 2000.

Woodruff, S.D., R.J. Slutz, R.L. Jenne and P.M. Steurer, A comprehensive ocean-atmosphere dataset, *Bull. Amer. Meteor. Soc., 68*, 521-527, 1987.

Xie, S.-P., T. Kunitani, A. Kubokawa, M. Nonaka, and S. Hosoda, Interdecadal thermocline variability in the North Pacific for 1958-1997: A GCM simulation, *J. Phys. Oceanogr., 30*, 2798-2813, 2000.

Xie, S.-P. , J. Hafner, Y. Tanimoto, W. T. Liu , H. Tokinaga and H. Xu, Bathymetric Effect on the Winter Climate of the Yellow and East China Seas, *Geophys. Res. Lett.*, doi:10.1029/2002GL015884R, in press, 2002.

Xie, S.-P., and M. Seki, Causes of equatorial asymmetry in sea surface temperature over the eastern Pacific, *Geophys. Res. Lett., 24,* 2581-2584, 1997.

Zhang, Y., J. M. Wallace and D.S. Battisti, ENSO-like interdecadal variability: 1900-93, *J. Clim., 10*, 1004-1020, 1997.

Y. Tanimoto, Frontier Research System for Global Change, Yokohama 236-0001, Japan and Graduate School of Environmental Earth Science, Hokkaido University, Sapporo 060-0810, Japan. (tanimoto@ees.hokudai.ac.jp)

H. Nakamura, Frontier Research System for Global Change, Yokohama 236-0001, Japan and Department of Earth and Planetary Science, University of Tokyo, Tokyo 113-0033, Japan. (hisashi@eps.s.u-tokyo.ac.jp)

T. Kagimoto and S. Yamane, Frontier Research System for Global Change, Yokohama 236-0001, Japan. (kagimoto@jamstec.go.jp, yamane@jamstec.go.jp)

(Received December 18, 2002; revised April 23, 2003;
accepted *** **, 2003.)

Paper number 2003JA900000.
****-****/**/2003JA900000$09.00

Figure 1. (a) Map of local cross-correlation between DJF-mean scalar wind speed ($U_a^{'}$) contribution as a component of linearized turbulent heat flux anomalies and JFM-mean SSTA in the North Pacific. (b) Same as in (a), but for SATA contribution (DJF) and SSTAs (JFM). Note that the former is negatively proportional to SATA. (c) Same as in (a), but for the total linearized flux anomalies (DJF) and SSTAs (JFM). In (c), a region [35~45°N, 140~165°E] of the positive correlation is indicated by an inset rectangle. Coloring convention is represented at the bottom of panel.

Figure 1. (a) Map of local cross-correlation between DJF-mean scalar wind speed ($U_a^{'}$) contribution as a component of linearized turbulent heat flux anomalies and JFM-mean SSTA in the North Pacific. (b) Same as in (a), but for SATA contribution (DJF) and SSTAs (JFM). Note that the former is negatively proportional to SATA. (c) Same as in (a), but for the total linearized flux anomalies (DJF) and SSTAs (JFM). In (c), a region [35~45°N, 140~165°E] of the positive correlation is indicated by an inset rectangle. Coloring convention is represented at the bottom of panel.

Figure 2. (a) Same as in Figure 1, but for the reversed lead-lag relationship.

Figure 2. (a) Same as in Figure 1, but for the reversed lead-lag relationship.

Figure 3. Map of local cross-correlation between DJF mean scalar wind speed and JFM mean SATA in the North Pacific. Contour lines (interval: 4°C) of the climatological DJF-mean SAT are superimposed.

Figure 3. Map of local cross-correlation between DJF mean scalar wind speed and JFM mean SATA in the North Pacific. Contour lines (interval: 4°C) of the climatological DJF-mean SAT are superimposed.

Figure 4. (a-c); Difference maps of bi-monthly SSTAs (°C) associated with the dominant mode of the North Pacific decadal climate variability between the two 4-year periods of 1968/69-1971/72 (category DC+) and 1982/83-85/86 (category DC-; i.e., DC+ minus DC-) for the (a) November-December, (b) January-February and (c) March-April periods. (d-f); As in (a-c), respectively, but for the difference maps for the ENSO-related SSTAs, based on the composite for 1967/68, 70/71,73/74, 84/85 winters (category IA+) and 1969/70, 72/73, 82/83, 87/88 winters (category IA-; i.e., IA+ minus IA-). Coloring convention is represented at the bottom of panel.

Figure 4. (a-c); Difference maps of bi-monthly SSTAs (°C) associated with the dominant mode of the North Pacific decadal climate variability between the two 4-year periods of 1968/69-1971/72 (category DC+) and 1982/83-85/86 (category DC-; i.e., DC+ minus DC-) for the (a) November-December, (b) January-February and (c) March-April periods. (d-f); As in (a-c), respectively, but for the difference maps for the ENSO-related SSTAs, based on the composite for 1967/68, 70/71,73/74, 84/85 winters (category IA+) and 1969/70, 72/73, 82/83, 87/88 winters (category IA-; i.e., IA+ minus IA-). Coloring convention is represented at the bottom of panel.

Figure 5. Difference maps of surface wind velocity (arrows) and scalar wind speed (colors; unit: m s^{-1}) between the categories DC+ and DC- (i.e., DC+ minus DC-) for the bi-monthly periods of (a) December-January and (b) February-March. These bi-monthly periods have been selected in

such a way that the wind forcing could correspond to SSTA tendencies between Figures 4a and 4b and between Figures 4b and 4c. Scaling of arrows (unit: m s^{-1}) is given at the bottom of each panel. Coloring convention is represented at the bottom of panel.

Figure 5. Difference maps of surface wind velocity (arrows) and scalar wind speed (colors; unit: m s^{-1}) between the categories DC+ and DC- (i.e., DC+ minus DC-) for the bi-monthly periods of (a) December-January and (b) February-March. These bi-monthly periods have been selected in such a way that the wind forcing could correspond to SSTA tendencies between Figures 4a and 4b and between Figures 4b and 4c. Scaling of arrows (unit: m s^{-1}) is given at the bottom of each panel. Coloring convention is represented at the bottom of panel.

Figure 6. Same as in Figure 5, but for the (a, b) total upward latent heat flux anomalies, (c, d) SSTA contribution, (e, f) SATA contribution, and (g, h) scalar wind speed contribution to (a, b), respectively (unit: W m^{-2}). An inset rectangle in each of (a)-(d) indicates the domain [35~45°N, 140~165°E], as in Figures 1c and 2c.

Figure 6. Same as in Figure 5, but for the (a, b) total upward latent heat flux anomalies, (c, d) SSTA contribution, (e, f) SATA contribution, and (g, h) scalar wind speed contribution to (a, b), respectively (unit: W m^{-2}). An inset rectangle in each of (a)-(d) indicates the domain [35~45°N, 140~165°E], as in Figures 1c and 2c.

Figure 7. Same as in Figure 5, but for difference maps between the categories IA+ and IA- (i.e., IA+ minus IA-).

Figure 7. Same as in Figure 5, but for difference maps between the categories IA+ and IA- (i.e., IA+ minus IA-).

Figure 8. Same as in Figure 6, but for difference maps between the categories IA+ and IA- (i.e., IA+ minus IA-).

Figure 8. Same as in Figure 6, but for difference maps between the categories IA+ and IA- (i.e., IA+ minus IA-).

Figure 9. Difference maps of (a) a wave-activity flux (arrows; unit: m^2s^{-2}), (b) storm track activity (colored; unit: K m s^{-1}), and (c) geopotential height tendency as a measure of feedback forcing from the storm track (colored; unit: m day^{-1}) between the categories DC+ (1968/69-1971/72) and DC- (1982/83-85/86) for December-January period. In (a) and (c), a difference map of 250-hPa geopotential height (unit: m) is superimposed by contour lines with 20 (m) intervals. The wave-activity flux in (a) has been evaluated from 250-hPa anomalous geostrophic streamfunction and corresponding wind anomalies using a formula of *Takaya and Nakamura* [2001]. The storm track activity in (b) is measured as the 850-hPa meridional heat flux associated with subweekly disturbances [*Nakamura et al.*, 2002]. The 250-hPa geopotential height tendency in (c) has been calculated solely from the vorticity flux convergence associated with subweekly disturbances at the same level [*Nakamura et al.*, 1997b]. Scaling of arrows is given at the top. Coloring convention is represented at the bottom of each panel.

Figure 9. Difference maps of (a) a wave-activity flux (arrows; unit: m^2s^{-2}), (b) storm track activity (colored; unit: K m s^{-1}), and (c) geopotential height tendency as a measure of feedback forcing from the storm track (colored; unit: m day^{-1}) between the categories DC+ (1968/69-1971/72) and DC- (1982/83-85/86) for December-January period. In (a) and (c), a difference map of 250-hPa geopotential height (unit: m) is superimposed by contour lines with 20 (m) intervals. The wave-activity flux in (a) has been evaluated from 250-hPa anomalous geostrophic streamfunction and corresponding wind anomalies using a formula of *Takaya and Nakamura* [2001]. The storm track activity in (b) is measured as the 850-hPa meridional heat flux associated with subweekly disturbances [*Nakamura et al.*, 2002]. The 250-hPa geopotential height tendency in (c) has been calculated solely from the vorticity flux convergence associated with subweekly disturbances at the same level [*Nakamura et al.*, 1997b]. Scaling of arrows is given at the top. Coloring convention is represented at the bottom of each panel.

Figure 10. (a, b) Same as in Figures 6a and 6b, respectively, but for the latent heat flux based on the NCEP/NCAR re-analyses.

Figure 10. (a, b) Same as in Figures 6a and 6b, respectively, but for the latent heat flux based on the NCEP/NCAR reanalyses.

TANIMOTO ET AL.: SST-HEAT FLUX RELATION

TANIMOTO ET AL.: SST-HEAT FLUX RELATION

TANIMOTO ET AL.: SST-HEAT FLUX RELATION

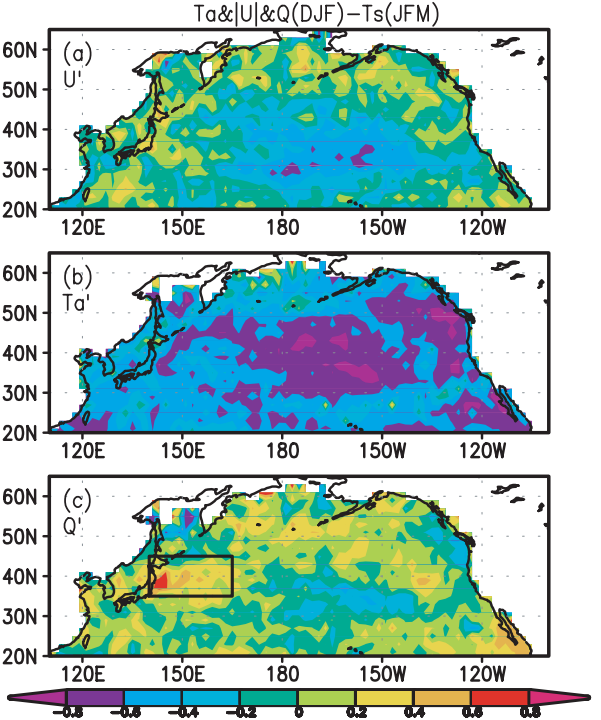

Figure 1. (a) Map of local cross-correlation between DJF-mean scalar wind speed (U_a) contribution as a component of linearized turbulent heat flux anomalies and JFM-mean SSTA in the North Pacific. (b) Same as in (a), but for SATA contribu-tion (DJF) and SSTAs (JFM). Note that the former is negatively proportional to SATA. (c) Same as in (a), but for the total linearized flux anomalies (DJF) and SSTAs (JFM). In (c), a region [35~45^{o}N, 140~165^{o}E] of the positive correlation is indicated by an inset rectangle. Coloring convention is represented at the bottom of panel.

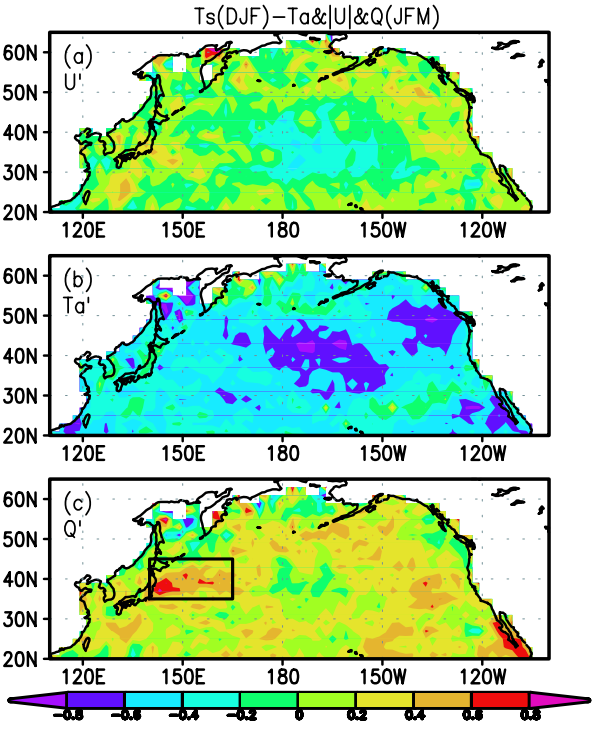

Figure 2. (a) Same as in Figure 1, but for the reversed lead-lag relationship.

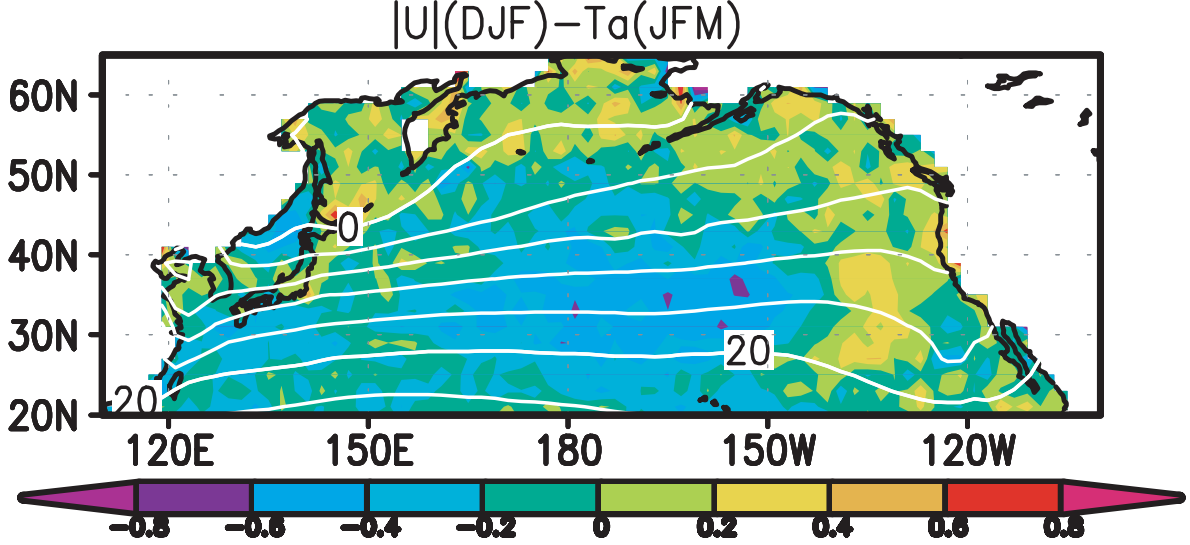

Figure 3. Map of local cross-correlation between DJF mean scalar wind speed and JFM mean SATA in the North Pacific. Contour lines (interval: 4^{o}C) of the climatological DJF-mean SAT are superimposed.

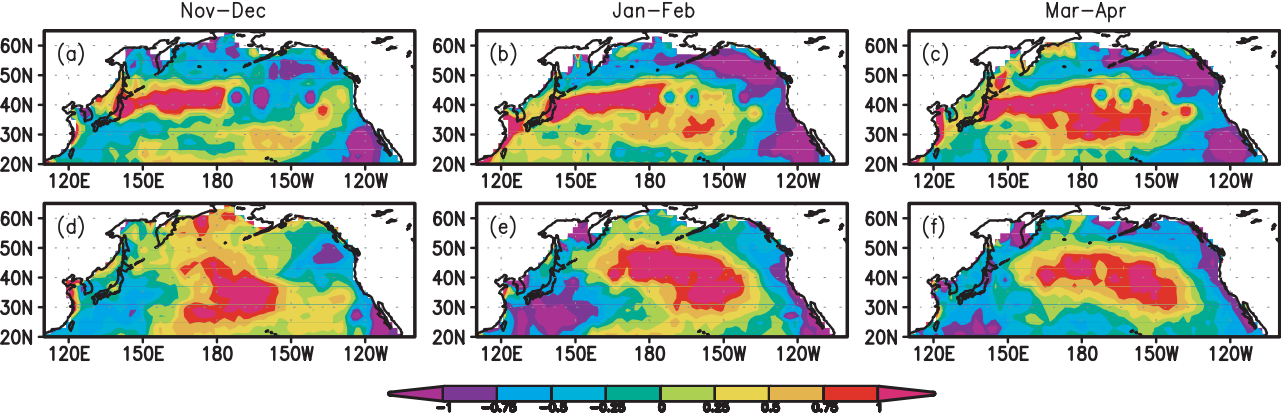

Figure 4. (a-c); Difference maps of bi-monthly SSTAs (^{O}C) associated with the dominant mode of the North Pacific decadal climate variability between the two 4-year periods of 1968/69-1971/72 (category DC+) and 1982/83-85/86 (category DC-; i.e., DC+ minus DC-) for the (a) November-December, (b) January-February and (c) March-April periods. (d-f); As in (a-c), respectively, but for the difference maps for the ENSO-related SSTAs, based on the composite for 1967/68, 70/71,73/74, 84/85 winters (category IA+) and 1969/70, 72/73, 82/83, 87/ 88 winters (category IA-; i.e., IA+ minus IA-). Coloring convention is represented at the bottom of panel.

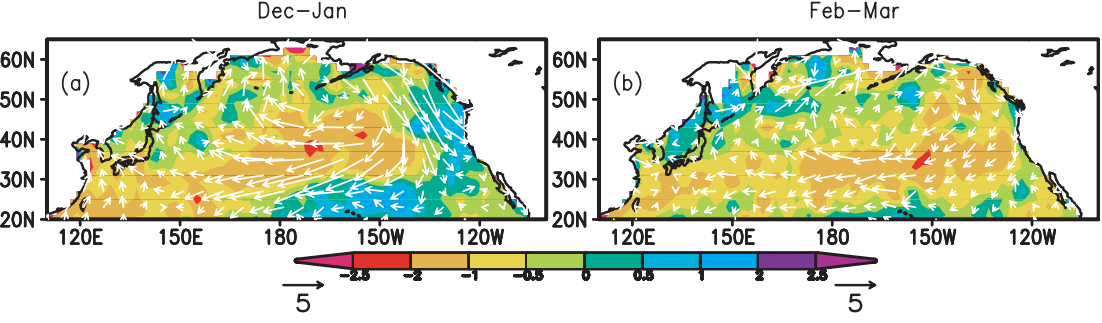

Figure 5. Difference maps of surface wind velocity (arrows) and scalar wind speed (colors; unit: m s^{-1}) between the categories DC+ and DC- (i.e., DC+ minus DC-) for the bi-monthly periods of (a) December-January and (b) February-March. These bi-monthly periods have been selected in such a way that the wind forcing could correspond to SSTA tendencies between Figures 4a and 4b and between Figures 4b and 4c. Scaling of arrows (unit: m s^{-1}) is given at the bottom of each panel. Coloring convention is represented at the bottom of panel.

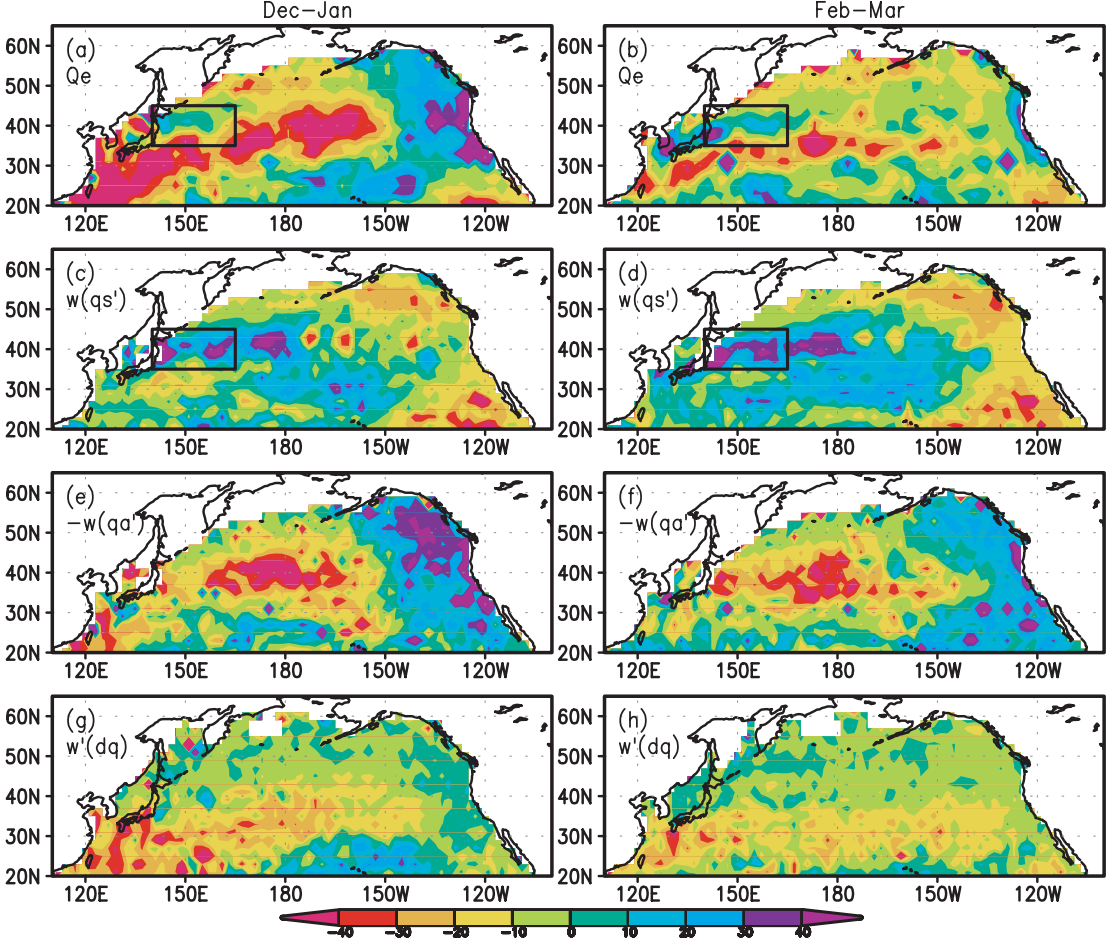

Figure 6. Same as in Figure 5, but for the (a, b) total upward latent heat flux anomalies, (c, d) SSTA contribution, (e, f) SATA contribution, and (g, h) scalar wind speed contribution to (a, b), respectively (unit: W m^{-2}). An inset rectangle in each of (a)-(d) indicates the domain [35~45^{o}N, 140~165^{o}E], as in Figures 1c and 2c.

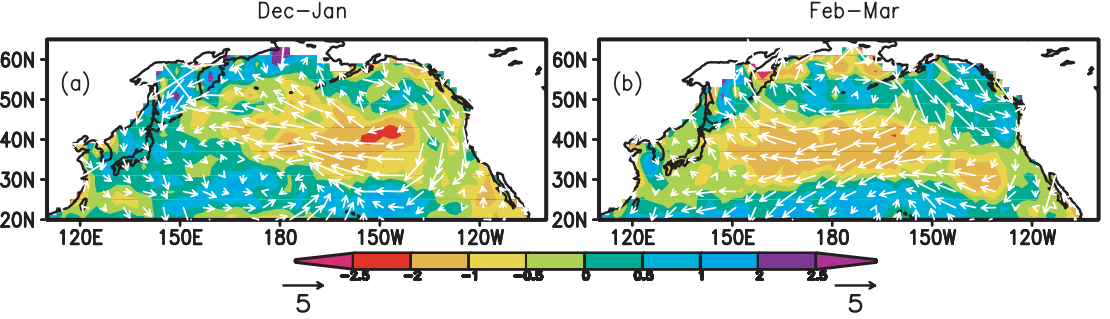

Figure 7. Same as in Figure 5, but for difference maps between the categories IA+ and IA- (i.e., IA+ minus IA-).

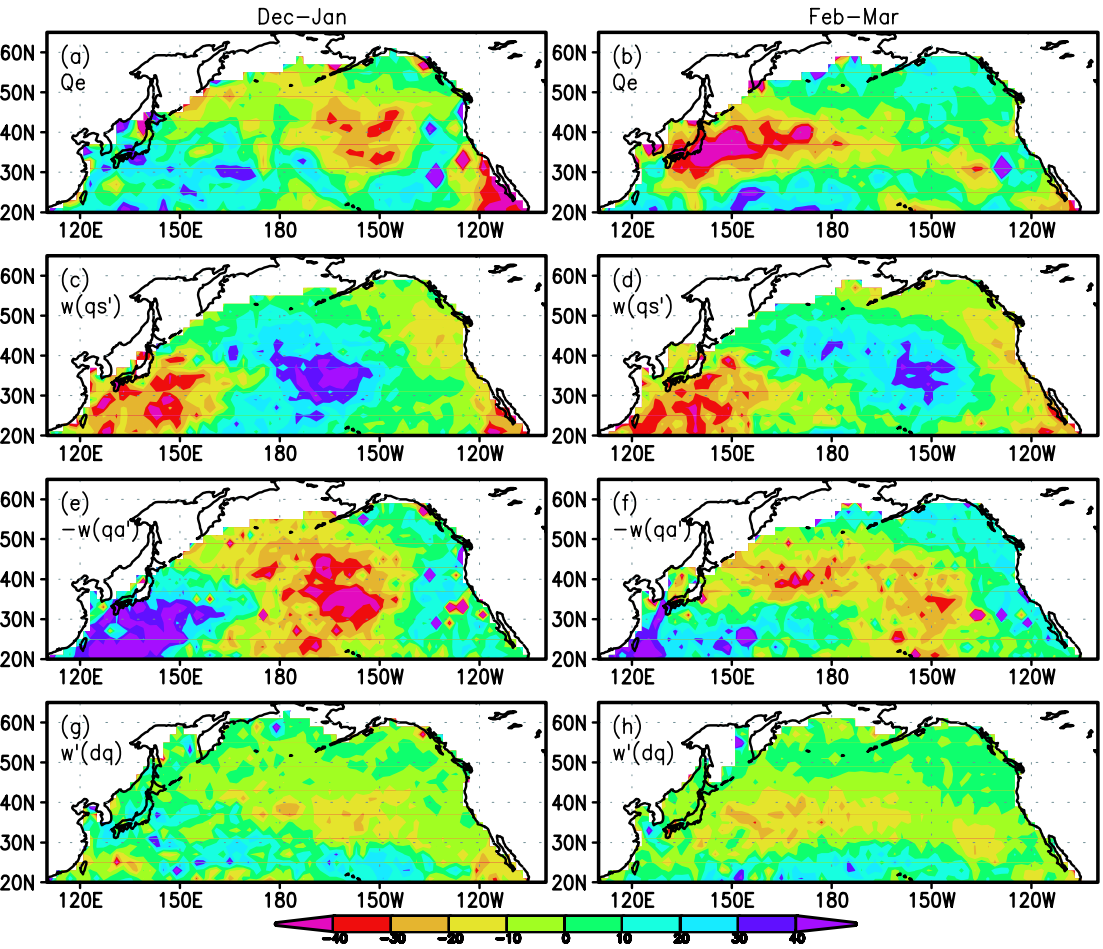

Figure 8. Same as in Figure 6, but for difference maps between the categories IA+ and IA- (i.e., IA+ minus IA-).

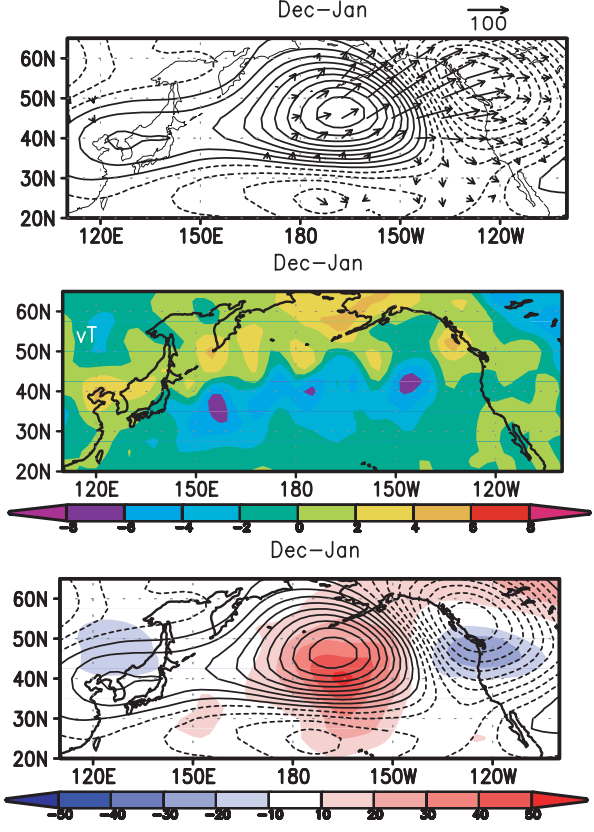

Figure 9. Difference maps of (a) a wave-activity flux (arrows; unit: m^2s^{-2}), (b) storm track activity (colored; unit: K m s^{-1})), and (c) geopotential height tendency as a measure of feedback forcing from the storm track (colored; unit: m day^{-1}) between the categories DC+ (1968/69-1971/72) and DC- (1982/83-85/86) for December-January period. In (a) and (c), a difference map of 250-hPa geopotential height (unit: m) is superimposed by contour lines with 20 (m) intervals. The wave-activity flux in (a) has been evaluated from 250-hPa anomalous geostrophic streamfunction and corresponding wind anomalies using a formula of *Takaya and Nakamura* [2001]. The storm track activity in (b) is measured as the 850-hPa meridional heat flux associated with subweekly disturbances [*Nakamura et al.*, 2002]. The 250-hPa geopotential height tendency in (c) has been calculated solely from the vorticity flux convergence associated with subweekly disturbances at the same level [*Nakamura et al.*, 1997b]. Scaling of arrows is given at the top. Coloring convention is represented at the bottom of each panel.

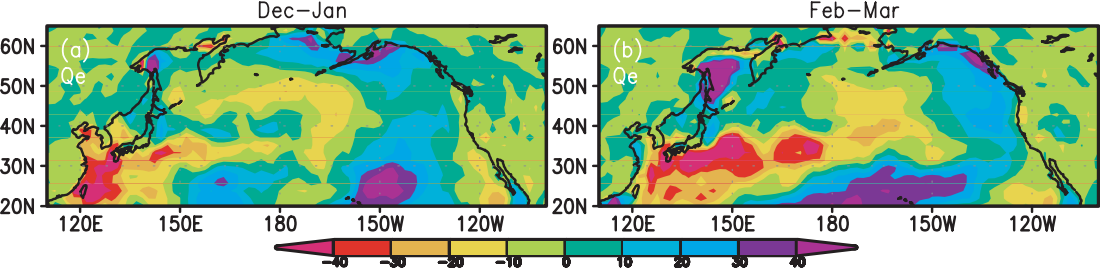

Figure 10. (a, b) Same as in Figures 6a and 6b, respectively, but for the latent heat flux based on the NCEP/NCAR reanalyses.